XXI IMEKO World Congress "Measurement in Research and Industry"
August 30 – September 4, 2015, Prague, Czech Republic

PLANAR MAGNETOSTATIC MODEL OF SOFT MAGNETIC OBJECTS IN HOMOGENEOUS MAGNETIC FIELD OF AN NMR IMAGER

I. Frollo, A. Krafčík, P. Andris, J. Přibil, and T. Dermek

Institute of Measurement Science, Slovak Academy of Sciences, Bratislava, Slovakia,
{ivan.frollo}@savba.sk

Abstract – Liquid samples with magnetic particles ingredients were placed into the homogenous magnetic field of an imager based on nuclear magnetic resonance. Theoretical computations based on a magnetostatic models were performed. For experimental verification an MRI 0.2 Tesla ESAOTE Opera imager was used. For modelling and experiments two samples - rectangular and circular were tested. The resultant images corresponds to the magnetic field variations in the vicinity of the samples.

Keywords: magnetic resonance imaging, mathematical modelling, magnetic liquids, magnetic susceptibility

1. INTRODUCTION

It is known from the physics, that every physical or biological object, which is inserted into magnetic field, deforms this field. Objects attract or detract the magnetic line of force, depending on the object substance: ferromagnetic, paramagnetic or diamagnetic.

The specific quantity is the magnetic susceptibility, that is defined as a change of magnetization in dependence on intensity magnetic field. Values of susceptibility defined as $\chi_i = (dM/dH)_0$ i.e. the slope at the origin, (M - magnetization, H - magnetic field, whereas $M = \chi H$) range from around -10^{-5} in very weak magnetic materials up to values of around $+10^6$ in ultra-soft ferromagnets [1], [2].

Imaging methods based on magnetic resonance principles are capable to detect, to measure and to image these deformations [3], [4], [5]. It is however very complicated to model such a situation and to compare a mathematical model with an image gained by a tomography. To this purpose mathematical models based on integral equations using scalar potential are applied. The calculation results are in a form of analytical expressions that for particular evaluation need perfect computational system and considerable computing time [6].

In this paper we try to describe the magnetic field distribution by mathematical modelling with an orientation to the simplest rectangular and circular objects.

For imaging a classical gradient-echo method, susceptible to magnetic field inhomogeneities, was used. The measurement sequence was specifically designed for to image the samples with maximal amplitude resolution.

2. THEORETICAL ANALYSIS

Let us assume that a ferromagnetic or paramagnetic object is placed into the homogeneous magnetic field of an MRI imager, the homogeneous magnetic field near the sample is deformed. For simplicity and easy experimental verification a double rectangular and circular objects were selected and theoretically analyzed.

A. Rectangular Sample

For the purpose of our simple example we suppose that the soft magnetic planar layer is positioned in the *x-y* plane of the rectangular coordinate system. This planar layer corresponds to transversal cross-section of a structure with an infinite depth or finite depth much more greater than dimensions of the layer (planar approximation).

According to Fig. 1, we suppose the layers are limited by dimensions of 2a and b, with the left-right symmetry. The layers are moved in y direction by distances +c and –c, $ds(x_1,y_1)$ is an elementary surface element. The basic magnetic field with flux density $\mathbf{B}_0$ of the MR imager is parallel with the y-axis. The task is to calculate the $\mathbf{B}(x,y,0)$ the magnetic flux density in the point A=[x,y,0].

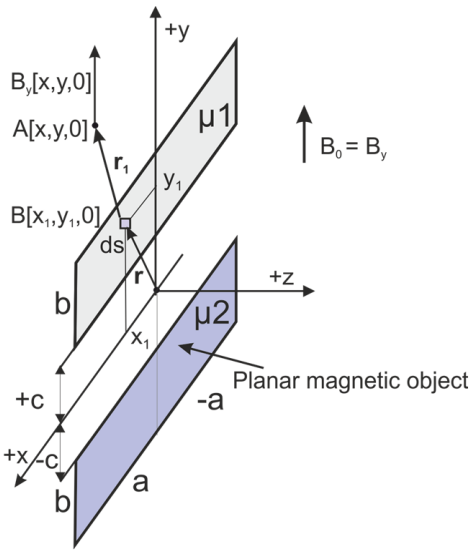

Fig. 1. Basic configuration of the magnetic planar rectangular layers. Samples are positioned in *x-y* plane of the rectangular coordinate system.

In planar approximation static magnetic objects (linear and isotropic) without any driving current can be described by Laplace equation

$$\nabla^2 A(x,y,z) = 0\,, \tag{1}$$

for nonzero z-component (A) of magnetic vector potential $\mathbf{A}=[0,0,A]$ and by boundary conditions at each interface between two media

$$\begin{aligned} \mathbf{n}_{\mathrm{II}} \cdot (\mathbf{B}_{\mathrm{I}} - \mathbf{B}_{\mathrm{II}}) &= 0, \\ \mathbf{n}_{\mathrm{II}} \times (\mathbf{H}_{\mathrm{I}} - \mathbf{H}_{\mathrm{II}}) &= \mathbf{0}, \end{aligned} \tag{2}$$

(e.g. material domains I and II, and $\mathbf{n}_{\mathrm{II}}$ is an outward normal from domain II), and outer boundary condition

$$\mathbf{B}\big|_{|\mathbf{r}|\to\infty} = \mathbf{B}_0\,. \tag{3}$$

Laplace equation is solvable analytically only for the simplest problems. For rectangular sample, these equations were therefore solved numerically by finite element method (FEM) using FEMM v.4.2 (D. Meeker). In this way it was calculated distribution of magnetic flux density field of two parallel bars with rectangular cross-section in x-y plane, with constant permeability μ_k (i.e. for k-th bar material domain) in originally homogeneous magnetic field with flux density $\mathbf{B}_0=[0,B_0,0]$ perpendicular to longitudinal axis of bars, see Fig. 2, obtained with FEM.

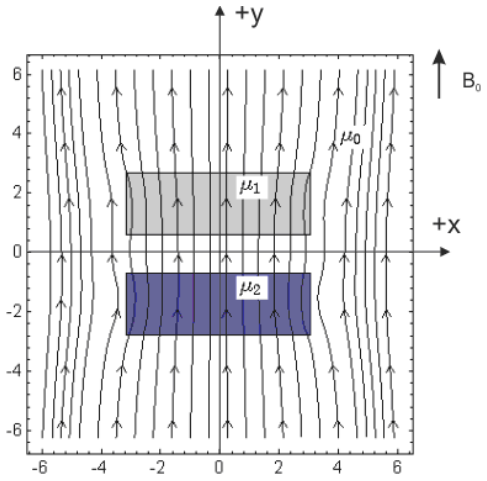

Fig. 2. Calculated magnetic field distribution of originally homogeneous magnetic field with magnetic flux density $\mathbf{B}_0$, lines of force, affected by 2 parallel magnetic bars with relative permeabilities: μ_1=2 , μ_2=3, environment permeability: μ_0.

In Fig. 3 and Fig. 4 you can see contour and surface plot of its magnetic flux density, obtained with FEM.

For experimental evaluation of the mathematical modelling, we have chosen a simple laboratory arrangement by application of the magnetic resonance imaging methods.

For sample positioning, a rectangular plastic vessel or holder with tap water was used. Two samples - rectangular

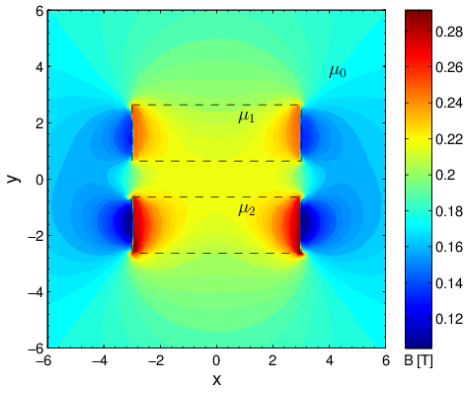

Fig. 3. Magnetic flux density of originally homogeneous magnetic filed affected by 2 parallel bars shown as contour plot. (Obtained with FEM.)

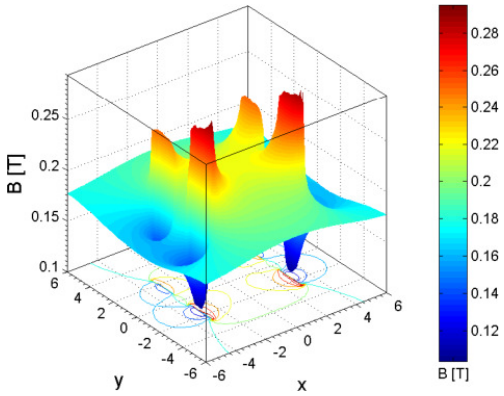

Fig. 4. Magnetic flux density of originally homogeneous magnetic filed affected by 2 parallel bars shown as surface plot. (Obtained with FEM.)

vessels filled with doped water (several drops of magnetic liquid based on Dextran) were placed to the centre of the holder. Dimensions of the samples: 50x10 mm^2, distance between samples: 5 mm. Thickness of the walls of sample vessels: 1 mm. Resultant image is in Fig. 5.

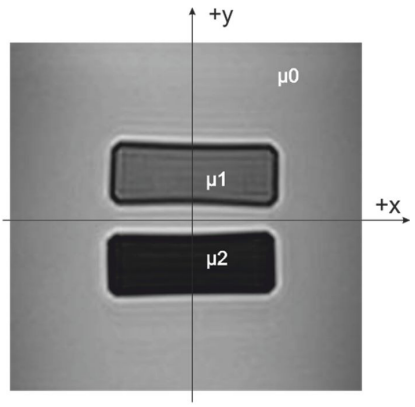

Fig. 5. NMR image of two samples (rectangular vessels filled with doped water in the holder with tap water) using GRE imaging sequence, TR = 440 ms, TE = 10 ms. Thickness of the imaged layer: 2 mm.

The contrast of the imaged samples corresponds to the real values of μ_1, μ_2, and μ_0. Walls of sample vessels with liquid substances are imaged with black colour, no MRI signal.

B. Circular Sample

For circular sample, 3 cylinder vessels placed in a rectangular plastic holder filled with the tap water were used. Cylinder vessels were filled with distilled water doped by several drops of magnetic liquid based on Dextran (polysaccharide).

According to Fig. 6, we suppose three circular concentric vessels. Relative permeabilities: μ_1, μ_2, and environment permeability: μ_0.

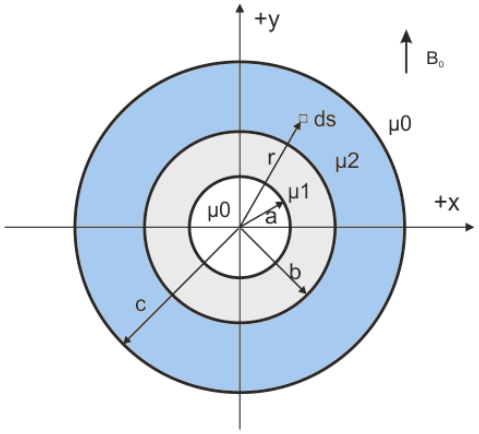

Fig. 6. Basic configuration of the magnetic planar layer circular sample positioned in *x-y* plane of the Cartesian coordinate system. (Cross-section of cylindrical vessels.)

From Fig. 6 the magnitude of position vector can be expressed in planar approximation as radial distance in cylindrical coordinate system

$$r = \rho \equiv \sqrt{x^2 + y^2}. \tag{4}$$

Thanks to the symmetry of configuration, Laplace equation (1) can be expressed in cylindrical coordinate system as

$$\begin{aligned} &\nabla^2 A(\rho,\varphi,z) \equiv \\ &\equiv \rho\frac{\partial^2 A}{\partial\rho^2} + \frac{\partial A}{\partial\rho} + \frac{1}{\rho}\frac{\partial^2 A}{\partial\varphi^2} + \frac{\partial^2 A}{\partial z^2} = 0, \end{aligned} \tag{5}$$

and solved analytically by separation of variables. For non-zero *z*-component of vector potential in *k*-th cylindrical layer or environment we can write [7]:

$$A_{\mathrm{k}} = \left(C_{\mathrm{k}}\rho + \frac{D_{\mathrm{k}}}{\rho}\right)\cos\varphi, \tag{6}$$

what yields radial and tangential components of magnetic flux density in the form

$$\begin{aligned} B_\rho^{\mathrm{k}} &= \frac{1}{\rho}\frac{\partial A_{\mathrm{k}}}{\partial\varphi} = -\left(C_{\mathrm{k}} + \frac{D_{\mathrm{k}}}{\rho^2}\right)\sin\varphi, \\ B_\varphi^{\mathrm{k}} &= -\frac{\partial A_{\mathrm{k}}}{\partial\rho} = -\left(C_{\mathrm{k}} - \frac{D_{\mathrm{k}}}{\rho^2}\right)\cos\varphi, \end{aligned} \tag{7}$$

where C_{k} and D_{k} are constants calculated for every region (domain). In material domain where $\rho = 0$, vector potential has to be finite, what is fulfilled only if $D\big|_{\rho=0} = 0$. In a similar way, for domain where $\rho \to \infty$ ($\mu = \mu_0$), magnetic field has the intensity same as original external homogeneous magnetic field, therefore $C\big|_{\rho\to\infty} = \mu_0 H_0$. Remaining constants can be determined from boundary conditions (2) on each cylindrical interface between two material domains (e.g. I and II with radius R_I), rewritten explicitly in the form

$$\begin{aligned} B_\rho^{\mathrm{I}}\big|_{\rho=R_{\mathrm{I}}} &= B_\rho^{\mathrm{II}}\big|_{\rho=R_{\mathrm{I}}}, \\ \frac{1}{\mu_{\mathrm{I}}} B_\varphi^{\mathrm{I}}\big|_{\rho=R_{\mathrm{I}}} &= \frac{1}{\mu_{\mathrm{II}}} B_\varphi^{\mathrm{II}}\big|_{\rho=R_{\mathrm{I}}}, \end{aligned} \tag{8}$$

Solution for configuration shown in Fig. 6 with relative permeabilities $\mu_1 = 2$ and $\mu_2 = 3$ yields:

$$\begin{aligned} C_{\mathrm{I}} &= -H_0 \frac{24b^2c^2\mu_0}{5a^2b^2 - 2a^2c^2 + 3b^4 - 30b^2c^2}, \\ D_{\mathrm{I}} &= 0, \\ C_{\mathrm{II}} &= -H_0 \frac{36b^2c^2\mu_0}{5a^2b^2 - 2a^2c^2 + 3b^4 - 30b^2c^2}, \\ D_{\mathrm{II}} &= H_0 \frac{12a^2b^2c^2\mu_0}{5a^2b^2 - 2a^2c^2 + 3b^4 - 30b^2c^2}, \\ C_{\mathrm{III}} &= -H_0 \frac{3c^2\mu_0(a^2 + 15b^2)}{5a^2b^2 - 2a^2c^2 + 3b^4 - 30b^2c^2}, \\ D_{\mathrm{III}} &= H_0 \frac{3c^2\mu_0(5a^2b^2 + 3b^4)}{5a^2b^2 - 2a^2c^2 + 3b^4 - 30b^2c^2}, \\ C_{\mathrm{IV}} &= \mu_0 H_0, \\ D_{\mathrm{IV}} &= H_0 \frac{c^2\mu_0(10a^2b^2 - a^2c^2 + 6b^4 - 15b^2c^2)}{5a^2b^2 - 2a^2c^2 + 3b^4 - 30b^2c^2}. \end{aligned} \tag{9}$$

Resultant *z*-component of vector potential respecting four regions using constants C_{I} to C_{IV} and D_{I} to D_{IV} in planar approximation is as follows:

$$A = \begin{cases} A_{\mathrm{I}}, & \text{for} \quad \rho \le \mathrm{a}, \\ A_{\mathrm{II}}, & \text{for} \quad a < \rho \le \mathrm{b}, \\ A_{\mathrm{III}}, & \text{for} \quad b < \rho \le \mathrm{c}, \\ A_{\mathrm{IV}}, & \text{for} \quad \mathrm{c} < \rho, \end{cases} \tag{10}$$

and vector potential **A**=[0,0,*A*]. Resultant flux density of magnetic field will be:

$$\mathbf{B} = \nabla \times \mathbf{A}\,. \qquad (11)$$

Its magnetic flux density lines is possible to draw as a stream plot, Fig. 7, relative values.

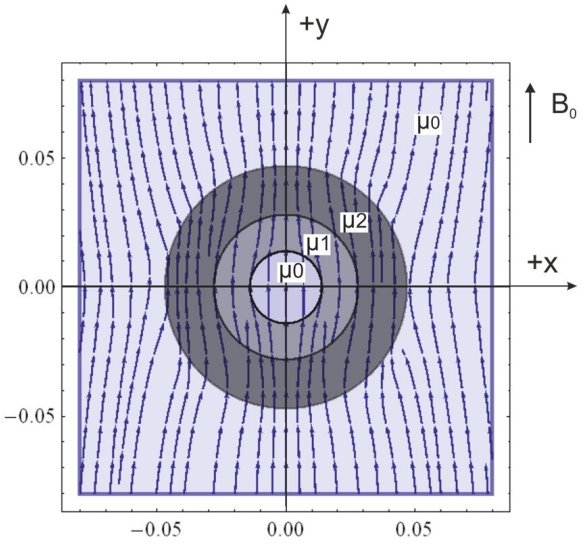

Fig. 7. Mathematical model of the distribution of homogeneous magnetic field $\mathbf{H}_0$, lines of force, affected by 2 concentric cylinders with relative permeabilities: μ_1=2 and μ_2=3, μ_0 is an environment permeability.

In Fig. 8 and Fig. 9 you can see contour and surface plot of its magnetic flux density, obtained with FEM.

For experimental evaluation of the mathematical modelling a rectangular plastic vessel - holder with tap water inside was chosen. Two samples - circular vessels filled with doped water were placed to the centre of the holder. The central vessel was filled with tap water. Diameters of the vessels: 18, 40, 56 mm, wall thickness: 1 mm. Resultant image is depicted in Fig. 10.

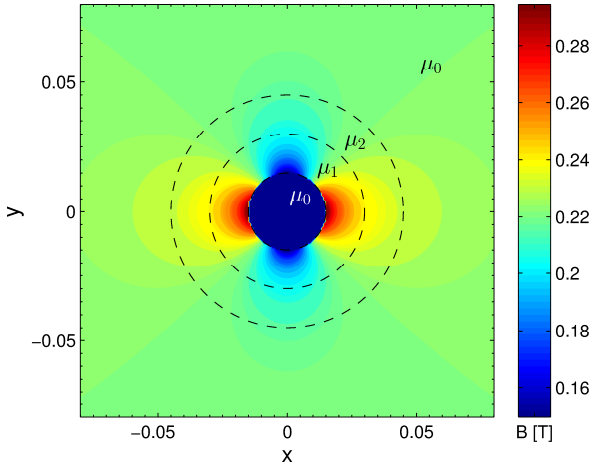

Fig 8. Magnetic flux density of originally homogeneous magnetic filed affected by 3 concentric cylinders shown as a contour plot.

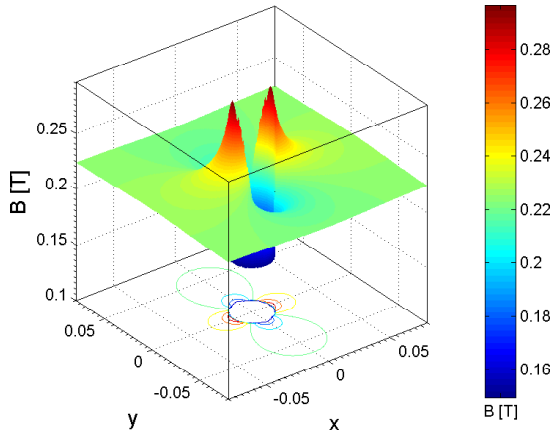

Fig 9. Magnetic flux density of originally homogeneous magnetic filed affected by 3 concentric cylinders shown as a surface plot.

For experimental verification an MRI 0.2 Tesla ESAOTE Opera imager (Esaote, Genoa, Italy) with vertical orientation of the basic magnetic field was used.

Several gradient-echo sequences were tested. It is evident, that every designed sequence is generating different image. We tried to find the best correlation between calculated results and resultant images.

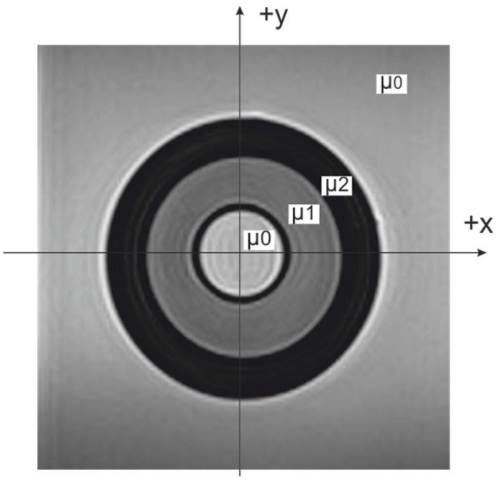

Fig. 10. NMR image of two samples (circular vessels filled with doped water in the rectangular vessels - holder filled with tap water) using GRE imaging sequence, TR = 440 ms, TE = 10 ms. Thickness of the imaged layer: 2 mm.

4. CONCLUSIONS

The goal of this study was to mathematically describe and experimentally image simple rectangular and circular objects - vessels filled with doped water by very diluted magnetic liquids. Imaging method based on MR principles was used for interpretation of analyzed samples.

Mathematical analysis of rectangular and circular objects, representing a shaped magnetic soft layer, showed theoretical possibilities to calculate magnetic field around any type of sample. Our mathematical model proved that it is possible to map the magnetic field variations - line of force - and to image the specific structures of selected

samples placed into a special plastic holders. The calculations were performed with relative values of input quantities, permeabilities and dimensions. The mathematical model was described in the form of general formulas. To present the detailed analytical form of resultant equations would exceed the range of this paper.

For experimental presentation a classical gradient echo measuring sequences were used.

The resultant MR images are encircled by narrow stripes that optically extend the width of the sample. This phenomenon is typical for susceptibility imaging, when one needs to measure local magnetic field variations representing sample properties [6].

Our experimental results are in good correlation with the mathematical simulations in spite of used relative quantities. This validates the possible suitability of the proposed method for detection of weak magnetic materials using the MRI methods. Presented images of thin objects indicate perspective possibilities of this methodology even in the low-field MRI.

ACKNOWLEDGMENTS

The work has been done in the framework of the COST project TD1103, and it has been supported by the Grant Agency of the Slovak Academy of Sciences VEGA 2/0013/14 and by the project of the Slovak Research and Development Agency Nr. APVV-0431-12.

REFERENCES

[1] É. Du Trémolet de Lacheisserie, D. Gignoux, and M. Schlenker, "*Magnetism: Fundamentals*", First Springer Science+Business Media, Inc. softcover printing, E-book ISBN 0-387-23062-9, 2005.

[2] Z.H.I. Sun, M. Guo, J. Vleugels, O. Van der Biest, B. Blanpain, "Processing of non-ferromagnetic materials in strong static magnetic field", *Current Opinion in Solid State and Materials Science,* vol. 17 , pp. 193–201, 2013.

[3] P. T. Callaghan, J. Stepisnik, "Spatially-distributed pulsed gradient spin echo NMR using single-wire proximity", *Physical Review Letters*, vol. 75, pp. 4532-4535, 1995.

[4] M. Sekino, T. Matsumoto, K. Yamaguchi, N. Iriguchi, S. Ueno, "A method for NMR imaging of a magnetic field generated by electric current", *IEEE Transactions on Magnetics*, vol. 40, pp. 2188-2190, 2004.

[5] E. M. Haacke, R. W. Brown, M. R. Thompson, R. Venkatesan, "*Magnetic Resonance Imaging: Physical Principles and Sequence Design*", first ed. Wiley-Liss, John Wiley and Sons Ltd, United States, 1999.

[6] P. Marcon, K. Bartusek, Z. Dokoupil, E. Gescheidtova, "Diffusion MRI: Mitigation of Magnetic Field Inhomogeneities", *Measurement Science Review*, vol. 12, nº. 5, pp. 205-212, 2012.

[7] H. Henke, "*Elektromagnetische Felder, Theorie und Anwendung*", ISBN 978-3-540-71004-2 3. Aufl. Springer Berlin Heidelberg New York, 2007.